2-Pyridylcyanoxime–NiII Clusters with Unusual Topologies: Lone-Pair–π Interactions and Magnetic Properties

Albert Escuer,*[a] Jordi Esteban,[a] Júlia Mayans,[a] and Mercè Font-Bardia[b]

[a] Departament de Química Inorgànica, Universitat de Barcelona, Av. Diagonal 645, 08028 Barcelona, Spain E-mail: albert.escuer@ub.edu
http://www.ub.edu/inorgani/recerca/MagMol/magmol.htm
[b] Department de Cristallografia, Mineralogia i Dipòsits, Universitat de Barcelona, Martí Franquès s/n, 08028 Barcelona, Spain

Three new complexes derived from the reaction of the 2-pyridylcyanoxime ligand (pyC{CN}NOH) with several non-carboxylate nickel salts have been structural and magnetically characterized.Thecompounds with the formula $[Ni_3(MeOH)_{2-}$ $(CF_3COO)(OH)(pyC\{CN\}NO)_4]$ (1), $[NaNi(tfacac)_3]_n$ (2; tfacac = 1,1,1-trifluoroacetylacetone), $[Ni_5(H_2O)_2(N_3)_2(pyC\{CN\}NO)_8]$ (3), and $[Ni_3(pyC\{CN\}NO)_5(pyC\{CN\}NOH)](BF4)$ (4) exhibit unusual topologies with a triangular $\{Ni_3(\mu_3$-OH)-$(pyC\{R'\}NO)_3\}^{2+}$ core for 1, vertex-shared triangles with a $\{Ni_5(\mu_{1,1}\text{-}N_3)_2(pyC\{CN\}NO)_6\}^{2+}$ core for 3, and a $\{Ni_3(pyC\ CN\}NO)_4\}^{2+}$ core for 4. Direct-current (DC) magnetic measurements performed in the 2–300 K temperature range reveal antiferromagnetic interactions induced by the μ_3-OR or oximato superexchange pathways and ferromagnetic interactions promoted by the azido bridges, thereby resulting in ground states S = 0, 3, and 1 for 1, 3, and 4, respectively. Supramolecular lone-pair–π-ring interactions are reported for the first time for the pyC{CN}NO– ligand and its importance in the crystal packing is discussed.

Introduction

Employing the 2-pyridyloximate family of ligands in 3D cluster chemistry has been widely studied over the last decade[1] owing to its ability to generate clusters of interest in a variety of research fields such as bioinorganic modelization, [2] catalysis,[3] design of selective receptors,[4] or molecular magnetism, often in the search for single-molecule magnet (SMM) response.[5]

The 2-pyridyloximate family of ligands (formed by 2-pyridylaldoxime or its methyl, phenyl, or pyridyl ketoxime derivatives) has a rich nickel chemistry that exhibits a large variety of topologies[6] and medium-large nuclearities up to Ni_{14}.[7] Among them, the 2-pyridylcyanoxime ligand [(pyC{CN}NOH), Scheme 1] possesses unique properties owing to the cyano substituent on the vicinal C atom to the oximate function: the cyano group induces larger acidity of the oxime (3–5 units of pKa with respect to ligands with other alkyl or aromatic substituents),[1] and this proved to be the only 2-pyridyloximate prone to generate μ_3-OR triangular derivatives in isolated or edge-/vertex-sharing triangles.[6f,6g,7i,8] Our previous work on this ligand was devoted to the preparation of a series of triangular-based complexes to provide magnetostructural correlations that can be useful to rationalize the response of larger aggregates.[8]

In the search for new derivatives of the pyC{CN}NOH ligand, we have explored the response of the ligand in noncarboxylate chemistry by employing two kinds of nickel sources as starting reagents: hexafluoro- and trifluoroacetylacetonate nickel complexes (hfacac and tfacac, respectively) and non-coordinating counteranions such as perchlorate or tetrafluoroborate. In this work we report the syntheses, structural characterization, and magnetic study of $[Ni_3(MeOH)_2(CF_3COO)(OH)(pyC\{CN\}NO)_4]$ (1), $[NaNi(tfacac)_3]_n$ (2), $[Ni_5(H_2O)_2(N_3)_2(pyC\{CN\}NO)_8]$ (3), and $[Ni_3(pyC\{CN\}NO)_5(pyC\{CN\}NOH)](BF_4)$ (4) complexes. In light of the resulting complexes, it is worth noting that the most convenient starting salts were those that contained inorganic anions when generating compounds 3 and 4. In contrast, solvolysis of hfacac decomposes the ligand to trifluoroacetate, and when starting from the $[Ni\text{-}(tfacac)_2]$ complex, coordination of the oximato ligand was not achieved. Analysis of the structural data pointed to the ability of the cyano group of the $pyC\{CN\}NO^-$ ligand to establish strong intermolecular lone-pair–aromatic-ring interactions, which have a relevant structural role in the crystal packing. Susceptibility measurements show moderately strong antiferromagnetic coupling for 1 and 4 and a ferromagnetic response for 3. Complex 1 is a new example of a μ_3-OH centered triangle, and its coupling parameters and S = 0 ground state have been correlated with related systems recently reported by us,[8] whereas 3 and 4 are tri- and pentanuclear derivatives with unusual topologies and spin ground states of S = 1 and S = 3, respectively.

Results and discussion

Structural Description

[Ni$_3$(MeOH)$_2$(CF$_3$COO)(OH)(pyC{CN}NO)$_4$]·2.5MeOH (1·2.5MeOH)

A view of the molecular structure and the labeled core of complex 1 is illustrated in Figure 1. Selected interatomic distances and angles are listed in Table 1. The core of this compound consists of a nearly isosceles arrangement of three NiII cations joined by one μ_3-OH ligand with the O atom placed 0.606(2) Å out of the Ni_3 plane. Two sides of the triangle are defined by single oximato bridges that link Ni(2) with Ni(1) and Ni(3), whereas the third side between Ni(1) and Ni(3) is defined by one oximato and one syn–syn carboxylato bridge. As a consequence of the different kind of bridges, the Ni(1)···Ni(3) distance and Ni(1)–O–Ni(3) bond angles are shorter than Ni(2)···Ni(1,3) distances and Ni(2)–O–Ni(1,3) angles, respectively (Table 1).

Ni(2) links two pyC{CN}NO– ligands (coordinated by their two N atoms), one O-oximato donor, and the central μ_3-OH group with a NiN_4O_2 environment. Ni(1) and Ni(3) are coordinated by one pyC{CN}NO– ligand (bonded through their two N atoms), the central μ_3-OH group, one O-oximato donor, one O-carboxylate atom, and one methanol molecule, thereby resulting in a NiN_2O_4 environment. Three bridging oximato ligands are coordinated in its 2.111 mode, whereas the fourth pyC{CN}NO– is bonded to Ni(2) in its 1.011 coordination mode.

The methanol molecules are involved in a wide set of intra- and intermolecular hydrogen bonds (Figure 1). One of the methanol molecules coordinated to Ni(1) establishes a strong intramolecular hydrogen bond with the deprotonated O atom of the nonbridging pyC{CN}NO– ligand, whereas the lattice methanol molecules generate strong intermolecular hydrogen bonds that involve the μ_3-OH group and the MeOH molecule coordinated to Ni(3), thereby resulting in a 1D arrangement of trimers along the a direction of the cell. Other intermolecular interactions (π–π and π–lone pair) will be discussed in a separate section.

[NaNi(tfacac)$_3$]n (2)

A labeled plot and selected interatomic distances and angles are reported in Figure 2 and Table 2, respectively. The structure consists of chains of sodium cations coordinated by means of the O donors of {Ni(tfacac)3}– units. Repetition of this motif generates a one-dimensional system in which the Na^+ and Ni^{2+} cations alternate along the chain. The three tfacac– ligands act as chelating ligands on the nickel ion and as bridging ligands with the two neighbor sodium cations, thus exhibiting its 3.22 coordination mode. The chains are packed in layers along the bc diagonals of the cell with a 53.4° angle between them (Figure 2). Relevant interchain interactions are not present.

[Ni$_5$(H$_2$O)$_2$(N$_3$)$_2$(pyC{CN}NO)$_8$]·2CH$_2$Cl$_2$ (3·2CH$_2$Cl$_2$)

A labeled plot and selected interatomic distances and angles for 3 are reported in Figure 3 and Table 3, respectively. The centrosymmetric structure of 3 consists of two vertex-sharing triangles [Ni(1,2,3) and symmetry-related Ni(1,2',3')] held together by six oximato and two azido bridges.

The pyC{CN}NO– ligands exhibit three different coordination modes. Four of them are linked in the 2.111 mode by linking Ni(1) with Ni(2,3), two pyC{CN}NO– ligands link the three nickel atoms by means of its 3.211 mode, and the two remaining pyC{CN}NO– ligands are coordinated only by their N atoms (1.011 mode). Ni–O–N–Ni torsión angles are low except for Ni(2)–N(8)–O(3)–Ni(3), which shows a value of 104.2(1)°, and therefore the Ni(2)···Ni(3) direction defines the larger side of the triangle (Table 3). Ni(1) and Ni(2) are linked by one additional μ1,1-azido bridge, and the coordination sites of Ni(3) are fulfilled with two water molecules, thereby resulting in an NiN_5O environment for Ni(1,2) and NiO_6 for Ni(3).

The water molecules coordinated to the central Ni(3) cation generate a set of intramolecular hydrogen bonds with the deprotonated 1.011 pyC{CN}NO– ligands and the N(15) atom of the azide ligands. Intermolecular π–π and π–lone-pair interactions will be discussed in a separate section.

$[Ni_3(pyC\{CN\}NO)_5(pyC\{CN\}NOH)](BF_4)\cdot 2CH_2Cl_2$ (4·2CH_2Cl_2)

A labeled plot of 4 is depicted in Figure 4, and selected interatomic distances and angles are listed in Table 4. The anionic triangular unit of 4 is formed by three Ni^{II} cations linked by six oximato bridges in a nearly isosceles arrangement. Each nickel cation links two pyC{CN}NO– ligands (coordinated by their two N atoms) and two O atoms from two bridging oximato groups, thereby resulting in an NiN_4O_2 environment for all of them. As in compound 1, two sides of the triangle are defined by two 2.111 pyC{CN}NO– ligands; but in contrast, the third side is defined by two 3.211 pyC{CN}NO– ligands in this case. As a consequence, Ni(2) is linked to Ni(1) and Ni(3) by means of a triple bridge (two oximates and one O donor), whereas Ni(1) and Ni(3) are linked by a double oximato bridge. The Ni(1)···Ni(3) side of the triangle exhibits the larger Ni···Ni distance as a consequence of the large Ni–N–O–Ni torsion angles between Ni(1)/Ni(3) (Table 4). The two remaining oximate ligands are coordinated to Ni(1) and Ni(3) in its 1.011 mode, but only one is deprotonated, thus forming a very strong intramolecular hydrogen bond between them. Intermolecular π–π and π–lone-pair interactions will be discussed in the next section.

Intramolecular Interactions

The importance of noncovalent interactions, mainly π–π stacking, has been widely recognized in biological systems, as it plays an essential role in protein folding or the stabilization of the DNA structure.[10] Electron-deficient aromatic π systems can also interact with anions, and their relevance has also been recognized in biological structures; as a consequence, this kind of supramolecular interaction has received considerable attention.[11] More recently, in addition to the anion–π interactions, lone-pair–π interactions between neutral molecules and aromatic rings have been demonstrated by both experimental and ab initio calculations.[12] These weak forces play a relevant role in crystal engineering because they often determine the crystal packing of the molecules. The pyridinic ring of the pyC{CN}NO– ligand is an electron-deficient aromatic ring, and complexes 1, 3, and 4 provide nice examples of a variety of intermolecular π interactions that will be described in detail in this section.

The main intermolecular interaction present in complex 1 consists of hydrogen bonds that involve solvate methanol molecules that determine the 1D arrangement along the a direction as was described above (Figure 1). However, analysis of the relative position of the pyC{CN}NO– ligands reveals additional intermolecular head-to-tail interactions between pairs of pyC{CN}NO– ligands: the deprotonated pyC{CN}NO– ligand coordinated to Ni(2) is placed parallel to the equivalent ligand of a

neighboring triangle with a distance between the N(11) nitrile atom and the centroid of the pyridinic ring of only 3.217 Å, thus generating pairs of dimers (Figure 5).

This pairs of dimers interact by means of conventional π–π contacts between the rings coordinated to Ni(3), with a distance of 3.291 Å between the rings (distance between centroids 3.725 Å), thus determining a zigzag 1D arrangement perpendicular to the a axis hydrogen-bond direction (Figure 6).

The pentanuclear compound 3 exhibits the same kind of head-to-tail interactions between pairs of equivalent ligands as compound 1. One of the pyC{CN}NO– ligands coordinated to Ni(1) establishes a contact with the neighboring molecule with a distance between the N(19) nitrile atom and the centroid of the pyridinic ring of 3.331 Å. This is the main intermolecular interaction for 3 and determines the supramolecular 1D arrangement of pentamers (Figure 5). The remaining pyridinic rings show several conventional π–π contacts that are directed roughly perpendicular to the chain that define the molecular packing in the crystal.

Compound 4 also shows one N(19) nitrile interaction with one pyridinic ring of the neighboring molecule with a distance of 3.484 Å to the centroid, which gives pairs of trimers (Figure 5). The tridimensional arrangement of these pairs of trimers in the crystal is directed by π–π interactions and one C–H/π-ring interaction with an H–centroid distance of 2.656 Å (Figure 7). Interestingly, the dichloromethane solvate molecules also interact with one of the pyridinic rings with distances Cl(1)–centroid of 3.913 Å and Cl(3)–centroid of 3.496 Å (Figure 7).

Magnetic Measurements and Modelization

The 1D compound 2 shows a practically constant $\chi_M T$ product between 300 and 6 K (around 1.27 $cm^3mol^{-1}K$) and only at very low temperature does it decrease to 1.06 $cm^3mol^{-1}K$. This response corresponds to non-interacting Ni^{2+} cations and it will not be discussed further. The temperature dependences of the $\chi_M T$ product for compounds 1, 3, and 4 are plotted in Figure 8.

Product of $\chi_M T$ for the triangular compounds 1 and 4 show values at room temperature (2.96 and 3.28 $cm^3mol^{-1}K$, respectively) close to the expected for three isolated Ni^{II} cations. On cooling, the $\chi_M T$ value decreases continuously and tends toward zero for 1 (χM maximum at 15 K) and to 1.05 $cm^3mol^{-1}K$ for 4. The magnetic behavior at low temperature is different but overall the plots evidence antiferromagnetic interactions for both compounds. Pentanuclear complex 3 shows a room-temperature value of the $\chi_M T$ product of 5.43 $cm^3mol^{-1}K$, slightly higher than the expected value for five isolated S = 1 centers. On cooling, $\chi_M T$ decreases to a minimum of 4.18 $cm^3mol^{-1}K$ at 35 K. Below this temperature $\chi_M T$ increases to a maximum value of 4.84 $cm^3mol^{-1}K$ at 5K, thus suggesting a ferrimagnetic response.

In light of the structural parameters and the topology of the complexes, the magnetic properties were modeled according to the coupling schemes shown in Scheme 2.

The fit of the experimental data was made using the PHI program.[13] On the basis of the roughly isosceles core of compounds 1 and 4, the two-*J* model schematized in Scheme 2 was assumed by applying the derived Hamiltonian [Equation (1)].

$$H = -J_1(S_1 \cdot S_2 + S_2 \cdot S_3) - J_2(S_1 \cdot S_3) \quad (1)$$

The best fit parameters were $J_1 = -41.0$ cm^{-1}, $J_2 = -29.8$ cm^{-1}, g = 2.24, and $R = 1.8\text{x}10^{-5}$ [$R = (\chi_M T_{exp} - \chi_M T_{calcd.})2/(\chi_M T_{exp.})2$] for 1 and $J_1 = -26.8$ cm–1, $J_2 = 2.0$ cm^{-1}, g = 2.21, and $R = 4.2\text{x}10^{-5}$ for 4.

The experimental data for compound 3 were fitted by applying the three-J Hamiltonian [Equation (2)].

$$H = -J_1(S_1 \cdot S_2 + S_1{\cdot\cdot}S_2{\cdot}) - J_2(S_1 \cdot S_3 + S_1{\cdot\cdot}S_3) - J_3(S_2 \cdot S_3 + S_2{\cdot\cdot}S_3) \quad (2)$$

and the best fit parameters were: $J_1 = 10.8$ cm^{-1}, $J_2 = -39.2$ cm^{-1}, $J_3 = 6.0$ cm^{-1}, g = 2.15, and $R = 1.1\text{x}10^{-5}$.

Magnetization at 2 K for 1 reaches negligible values, whereas for 3 and 4 the magnetization tends to quasi-saturated values equivalent to 5.2 and 2.0 electrons under the maximum external field of 5 T, which is in good agreement with the proposed ground states of S = 0, S = 3, and S = 1, respectively (Figure 8). Fitting of the magnetization data (at 2 K) gives $J_1 = 9.6$ cm^{-1}, $J_2 = -41.6$ cm^{-1}, $J_3 = 6.0$ cm^{-1}, $D_{ion} = 5.1$ cm^{-1}, g = 2.10, and $R = 3.3\text{x}10^{-4}$ for 3 and $J_1 = -25.6$ cm^{-1}, $J_2 = 2.0$ cm^{-1}, $D_{ion} = 3.2$ cm^{-1}, g = 2.21, and $R = 4.2\text{x}10^{-5}$ for 4, which is in excellent agreement with the susceptibility data.

The different ground state found for complexes 1 (S = 0) and 4 (S = 1) arises from their different J_1/J_2 ratio.[14] For an antiferromagnetically coupled triangle with three local S = 1 spins, there are competitive interactions or even spin frustration for the case $J_1/J_2 = 0.5$ or 2.0. For ratios lower than 0.5 or larger than 2.0, the ground state should be S = 1, but for ratios between 0.5 and 2.0 the ground state becomes S = 0 with a maximum stabilization for the ratio 1.0

($J_1 = J_2$, equilateral triangle). The J_1/J_2 ratio is 0.73 (S = 0) for 1 and –0.07 (S = 1) for complex 4, which leads to well-defined and isolated ground states as was observed experimentally.

The coupling constants calculated for compound 1 follow the correlation proposed on the basis of DFT calculations[8a] between the magnitude of the antiferromagnetic response and the Ni–O–Ni bond angles, which correlates the weaker interaction to the lower bond angle (–29.8 cm^{-1}/106.0°) and the stronger interaction to the larger angles (–41.0 cm–1/114.0–114.9°). The sign and magnitude of the superexchange interactions for the pentanuclear compound 3 also follow the expected general trends: ferromagnetic interaction[15] for the oximato/$\mu_{1,1}$-N_3 bridges between Ni(1) and Ni(2) and a moderate antiferromagnetic interaction mediated by oximato or oximato/oxo bridges that involves Ni(3). The obtained values are in good agreement with those reported for the only comparable system, [Ni_5(3-Cl-BzO)$_4$(6-mepao)$_4$(6-mepaoH)$_2$(N_3)$_2$], which was reported by us when employing the 6-methylpyridine-2-carbaldehyde oxime ligand (6-mepaoH).[6e]

In contrast, comparison of the magnetic response of the triangular topology of compound 4 with the available bibliographic data becomes surprising because no apparent correlation can be proposed. The main magneto-structural parameters for the reported complexes with the core shown in Scheme 3 are summarized in Table 5.

From Table 5 we can see that the general rule that postulates lower antiferromagnetic interactions for large Ni–N–O–Ni torsion angles[17] is followed for all compounds ($-J_1 > -J_2$). However, in light of the very similar values for the four reported compounds that exhibit this topology, all of the data are inconsistent. In fact, the Ni–O–Ni bond angles are practically identical and the minor changes in the τ1

241 torsion cannot justify the large variation in J_1, and the large range of J_2 for very similar τ_2 torsions is
242 surprising. Data collected in Table 5 suggest an unreliable fit of the coupling constants, but
243 magnetization experiments reported in this work confirm a thoroughly isolated S = 1 ground state (J_1/J_2
244 ratio of –0.07) for 4 and S = 0 ground state for BURSOX[16a] with a J_1/J_2 ratio of 0.60, thus offering
245 independent proof of the correct procedure in the susceptibility fitting process. The reason could be
246 attributable to electronic effects promoted by the different oximate ligands, but with the small amount
247 of experimental data it is speculative and additional compounds with this topology will be needed to
248 justify the apparently inconsistent *J* values

249

Conclusions

The 2-pyridylcyanoxime ligand has provided three new NiII systems with different topologies. From the synthetic point of view, it was observed that acetylacetonate NiII complexes easily decompose or displace the oximate ligand, as they are inadequate as starting reagents in contrast to inorganic salts or nickel carboxylates. Analysis of the magnetic data confirms the previously proposed antiferromagnetic interactions and their dependence of the Ni–O–Ni or Ni–N–O–Ni bond or torsion angles. Unprecedented lonepair–π-ring interactions between the cyano groups and the pyridinic rings have been identified and their influence in the crystal packing has been analyzed.

Experimental Section

General: 2-Pyridylacetonitrile and nickel acetate were purchased from Sigma–Aldrich Inc. and used without further purification. The pyC{CN}NOH ligand was prepared according to the improved[7i] method reported in the literature.[18] Samples for analyses were gently dried to remove volatile solvents. The yield for 1–4 was around 30% as a well-formed crystalline product, which was employed in the instrumental measures. Further powder fractions were discarded.

$[Ni_3(MeOH)_2(CF_3COO)(OH)(pyC\{CN\}NO)_4]\cdot 2.5MeOH$ (1· 2.5MeOH): 2-Pyridylcyanoxime (0.073 g, 0.5 mmol) was dissolved in MeOH (20 mL) together with $Ni(hfacac)_2\cdot H_2O$ (0.472 g, 1 mmol) and NEt_3 (0.101 g, 1.0 mmol). The solution was stirred for one hour, then filtered and left to crystallize in a closed vial. After one week, crystals adequate for X-ray determination were collected. As has often been observed, basic solvolysis of the hfacac ligands followed by a retro-Claisen condensation provides the trifluoroacetato ligand present in 1.[19] $C_{32}H_{25}F_3N_{12}Ni_3O_9$ (954.69): calcd. C 40.25, H 2.64, N 17.61; found C 39.2, H 2.7, N 17.5. Relevant IR bands: ν̃ = 3456 (br), 2223 (w), 1650 (s), 1602 (m), 1464 (s), 1430 (m), 1303 (w), 1257 (s), 1201 (m), 1150 (s), 1109 (w), 1039 (w), 781 (w), 712 (w), 672 (w) cm^{-1}.

$[NaNi(tfacac)_3]n$ (2): 2-Pyridylcyanoxime (0.147 g, 1.0 mmol) was dissolved in MeOH (30 mL) together with $Ni(tfacac)_2\cdot H_2O$ (0.362 g, 1 mmol), NaN3 (0.130 g, 2 mmol), and NEt3 (0.202 g, 2.0 mmol). The solution was stirred for one hour, then filtered and left to crystallize in a closed vial. In a few days, well-formed blue crystals were collected. Further evaporation of the resulting brown solution did not give any characterizable compound that contained the oximate ligand. $C_{15}H_{12}F_9NaNiiO_6$ (540.95): C 33.31, H 2.24; found C 33.6, H 2.1. Relevant IR bands: ν̃ = 1623 (s), 1477 (m), 1287 (s), 1134 (m), 861 (w), 578 (w) cm^{-1}.

$[Ni_5(H_2O)_2(N_3)_2(pyC\{CN\}NO)_8]\cdot 2CH_2Cl_2$ ($3\cdot 2CH_2Cl_2$): Reaction of $Ni(ClO_4)\cdot 6H_2O$ (0.360 g, 1 mmol) with 2-pyridylcyanoxime (0.073 g, 0.5 mmol), NaN_3 (0.065 g, 1 mmol), and Et_3N (0.101 g, 1 mmol) in dichloromethane (30 mL) gave a dark precipitate after stirring for 1 h. The precipitate was dissolved in hot dichloromethane and the solution was layered with diethyl ether to give wellformed crystals of compound 3. $C_{56}H_{36}N_{30}Ni_5O_{10}$ (1582.55): calcd. C 42.50, H 2.29, N 26.55; found C 41.8, H 2.4, N 25.9. Relevant IR bands: ν̃ = 3427 (br), 2217 (w), 2066 (s), 1602 (s), 1463 (s), 1218 (s), 1106 (m), 1029 (s), 777 (m), 707 (m) cm^{-1}.

$[Ni_3(pyC\{CN\}NO)_5(pyC\{CN\}NOH)](BF_4)\cdot 2CH_2Cl_2$ ($4\cdot 2CH_2Cl_2$): Performing the above reaction starting from $Ni(BF_4)\cdot 6H_2O$ (0.280 g, 1 mmol) instead of $Ni(ClO_4)\cdot 6H_2O$ by slow evaporation also yielded a first crystallization of compound 2. By monitoring the successive crops of crystals by IR spectroscopy (until complete extinction of the azide band), well-formed crystals of complex 4 could be collected. $C_{42}H_{25}BF_4N_{10}Ni_3O_6$ (1140.65): calcd. C 44.22, H 2.21, N 22.10; found C 43.2, H 2.4, N 21.5. Relevant IR bands: ν̃ = 3429 (br), 3072 (w), 2231 (w), 1602 (s), 1438 (m), 1228 (m), 1140 (m), 1109 (m), 1062 (s), 1026 (s), 1000 (w), 1036 (m), 777 (s), 743 (m), 707 (s) cm^{-1}.

Physical Measurements: Magnetic susceptibility measurements were carried out on polycrystalline samples with a Quantum Design MPMS-5 SQUID susceptometer working in the range 2–300 K under magnetic fields of 0.3 T (300–30 K) and 0.03 T (30–2 K) to avoid saturation effects. Diamagnetic

corrections were estimated from Pascal tables. Infrared spectra (4000–400 cm^{-1}) were recorded from KBr pellets with a Bruker IFS-125 FTIR spectrophotometer.

Single-Crystal X-ray Structure Analyses: Details of crystal data, data collection, and refinement are given in Table 6. X-ray data were collected with a Bruker APEX-II CCD diffractometer with a graphite monochromator for 1 and a D8 Venture system equipped with a multilayer monochromator and a Mo microfocus for 2, 3, and 4. The structure of 1 was solved by direct methods by using the SHELXS computer program[20] and refined by the full-matrix least-squares method with the SHELX97 computer program;[21] 27 hydrogen atoms were located from a difference synthesis and refined with an overall isotropic temperature factor, and six hydrogen atoms were computed and refined using a riding model with an isotropic temperature factor equal to 1.2 times the equivalent temperature factor of the atoms that are linked. The structures of compounds 2–4 were solved and refined using the Bruker SHELXTL software package and refined using SHELXL.[22] Three C atoms of one pyridinic ring (C9/C9′, C10/C10′, C11/C11′) and N19/N19′ of compound 3 were disordered with occupancy factors of 0.5. CCDC-1005347 (for 1), -1005348 (for 2), -1005349 (for 3), and -1005350 (for 4) contain the supplementary crystallographic data for this paper. These data can be obtained free of charge from The Cambridge Crystallographic Data Centre via www.ccdc.cam.ac.uk/data_request/cif.

320 **ACKNOWLEDGEMENTS**

321

322 Funds from the Ministerio de Economia y Competitividad (MEC) (project CTQ2012-30662) are
323 acknowledged. A. E. is thankful for financial support from the Excellence in Research ICREA-
324 Academia Award.

325

References

[1] C. J. Milios, T. C. Stamatatos, S. P. Perlepes, Polyhedron 2006, 25, 134–194.

[2] M. J. Goldcamp, S. E. Robison, J. A. Krause Bauer, M. J. Baldwin, Inorg. Chem. 2002, 41, 2307–2309.

[3] S. Akine, T. Taniguchi, T. Saiki, T. Nabeshima, J. Am. Chem. Soc. 2005, 127, 540–541.

[4] D. T. Rosa, J. A. Krause Bauer, M. J. Baldwin, Inorg. Chem. 2001, 40, 1606–1613.

[5] a) P. Chaudhuri, Coord. Chem. Rev. 2003, 243, 143–190; b) C. J. Milios, C. P. Raptopoulou, A. Terzis, F. Lloret, R. Vicente, S. P. Perlepes, A. Escuer, Angew. Chem. Int. Ed. 2004, 43, 210–212; Angew. Chem. 2004, 116, 212; c) C. J. Milios, E. Kefalloniti, C. P. Raptopoulou, A. Terzis, R. Vicente, N. Lalioti, A. Escuer, S. P. Perlepes, Chem. Commun. 2003, 819–821; d) C. J. Milios, T. C. Stamatatos, P. Kyritsis, A. Terzis, C. P. Raptopoulou, R. Vicente, A. Escuer, S. P. Perlepes, Eur. J. Inorg. Chem. 2004, 2885–2901; e) R. Clérac, H. Miyasaka, M. Yamashita, C. Coulon, J. Am. Chem. Soc. 2002, 124, 12837–12844.

[6] a) C. Papatriantafyllopoulou, G. Aromi, A. J. Tasiopoulos, V. Nastopoulos, C. P. Raptopoulou, S. J. Teat, A. Escuer, S. P. Perlepes, Eur. J. Inorg. Chem. 2007, 2761–2774; b) C. G. Efthymiou, A. A. Kitos, C. P. Raptopoulou, S. P. Perlepes, A. Escuer, C. Papatriantafyllopoulou, Polyhedron 2009, 28, 3177–3184; c) S. Zhang, L. Zhen, B. Xu, R. Inglis, K. Li, W. Chen, Y. Zhang, K. F. Konidaris, S. P. Perlepes, E. K. Brechin, Y. Li, Dalton Trans. 2010, 39, 3563–3571; d) H. Chen, C.-B. Ma, D.-Q. Yuan, M.-Q. Hu, H.-M. Wen, Q.-T. Liu, C.-N. Chen, Inorg. Chem. 2011, 50, 10342–10352; e) A. Escuer, G. Vlahopoulou, F. A. Mautner, Dalton Trans. 2011, 40, 10109–10116; f) J. Esteban, M. Font-Bardia, A. Escuer, Inorg. Chem. Commun. 2014, 43, 169–172; g) J. Esteban, M. Font-Bardia, J. Sanchez Costa, S. J. Teat, A. Escuer, Inorg. Chem. 2014, 53, 3194–3203.

[7] a) G. Psomas, C. Dendrinou-Samara, M. Alexiou, A. Tsohos, C. P. Raptopoulou, A. Terzis, D. P. Kessissoglou, Inorg. Chem. 1998, 37, 6556–6557; b) A. Pajunen, I. Mutikainen, H. Saarinen, M. Orama, Z. Kristallogr.-New Cryst. Struct. 1999, 214, 217–220; c) S. Khanra, T. Weyhermuller, E. Rentschler, P. Chaudhuri, Inorg. Chem. 2005, 44, 8176–8178; d) T. C. Stamatatos, E. Diamantopoulou, A. J. Tasiopoulos, V. Psycharis, R. Vicente, C. P. Raptopoulou, V. Nastopoulos, A. Escuer, S. P. Perlepes, Inorg. Chim. Acta 2006, 359, 4149–4157; e) T. C. Stamatatos, K. A. Abboud, S. P. Perlepes, G. Christou, Dalton Trans. 2007, 3861–3863; f) T. C. Stamatatos, A. Escuer, K. A. Abboud, C. P. Raptopoulou, S. P. Perlepes, G. Christou, Inorg. Chem. 2008, 47, 11825–11838; g) J. Esteban, L. Alcázar, M. Torres-Molina, M. Monfort, M. Font-Bardia, A. Escuer, Inorg. Chem. 2012, 51, 5503–5505; h) A. Escuer, J. Esteban, M. Font-Bardia, Chem. Commun. 2012, 48, 9777–9779; i) J. Esteban, M. Font-Bardia, A. Escuer, Inorg. Chem. 2014, 53, 1113–1121.

[8] a) J. Esteban, E. Ruiz, M. Font-Bardia, T. Calvet, A. Escuer, Chem. Eur. J. 2012, 18, 3637–3648; b) J. Esteban, M. Font-Bardia, A. Escuer, Eur. J. Inorg. Chem. 2013, 5274–5280.

[9] R. A. Coxall, S. G. Harris, D. K. Henderson, S. Parsons, P. A. Tasker, R. E. P. Winpenny, J. Chem. Soc., Dalton Trans. 2000, 2349–2356.

[10] a) S. K. Burley, G. A. Petsko, Science 1985, 229, 23–28; b) S. Li, V. R. Cooper, T. Thonhauser, B. I. Lundqvist, D. C. Langreth, J. Phys. Chem. B 2009, 113, 11166–11172.

[11] A. Frontera, P. Gamez, M. Mascal, T. J. Mooibroek, J. Reedijk, Angew. Chem. Int. Ed. 2011, 50, 9564–9583; Angew. Chem. 2011, 123, 9736 (review). Eur. J. Inorg. Chem. 2014, 5443–5450 5450 © 2014 Wiley-VCH Verlag GmbH & Co. KGaA, Weinheim

[12] a) T. J. Mooibroek, S. J. Teat, C. Massera, P. Gamez, J. Reedijk, Cryst. Growth Des. 2006, 6, 1569–1574; b) T. J. Mooibroek, P. Gamez, J. Reedijk, CrystEngComm 2008, 10, 1501–1515.

[13] N. F. Chilton, R. P. Anderson, L. D. Turner, A. Soncini, K. S. Murray, J. Comput. Chem. 2013, 34, 1164–1175.

[14] O. Kahn, Molecular Magnetism, VCH Publishers, New York, 1993, chapter 10.

[15] A. Escuer, J. Esteban, S. P. Perlepes, T. C. Stamatatos, Coord. Chem. Rev. 2014, 275, 87–129.

[16] a) C. G. Efthymiou, C. P. Raptopoulou, A. Terzis, S. P. Perlepes, A. Escuer, C. Papatriantafyllopoulou, Polyhedron 2010, 29, 627–633; b) V. V. Pavlishchuk, S. V. Kolotilov, A. W. Addison, M. J. Prushan, R. J. Butcher, L. K. Thompson, Inorg. Chem. 1999, 38, 1759–1766; c) T. Weyhermuller, R. Wagner, S. Khanra, P. Chaudhuri, Dalton Trans. 2005, 2539–2546.

[17] A. Escuer, J. Esteban, O. Roubeau, Inorg. Chem. 2011, 50, 8893–8901.

[18] a) N. N. Gerasimchuk, V. V. Skopenko, K. V. Domasevich, O. A. Zhmurko, Ukr. Khim. Zh. (Russ. Ed.) 1992, 58, 935–949; b) A. A. Mokhir, K. V. Domasevich, N. K. Dalley, X. Kou, N. N. Gerasimchuk, O. A. Gerasimchuk, Inorg. Chim. Acta 1999, 284, 85–98.

[19] a) S. R. Drake, A. Lyons, D. J. Otway, D. J. Williams, Inorg. Chem. 1994, 33, 1230–1233; b) S. Wang, Z. Pang, K. D. L. Smith, Y.-S. Yua, C. Deslippe, M. J. Wagner, Inorg. Chem. 1995, 34, 908–917.

[20] G. M. Sheldrick, SHELXS – A Computer Program for Determination of Crystal Structures, University of Göttingen, Germany, 1997.

[21] G. M. Sheldrick, SHELX97 – A Program for Crystal Structure Refinement, University of Göttingen, Germany, 1997.

[22] SHELXL, G. M. Sheldrick, Acta Crystallogr., Sect. A 2008, 64, 112–122.

Legends to figures

Scheme 1. 2-Pyridylcyanoxime ligand and coordination modes found in 1–4 (in Harris notation[9]) for the deprotonated pyC{CN}NO– ligand.

Figure 1. Top left: Molecular structure of compound 1. Top right: Labeled core of 1 showing the intramolecular hydrogen bond between the nonbridging oximate and the coordinated methanol molecule. Bottom: plot of the intermolecular hydrogen bonds involving the solvent molecules. Hydrogen bonds are shown as red dashed lines..

Figure 2. Left: Labeled asymmetric unit of compound 2. Right: Packing of the chains showing the layers of chains in two directions.

Figure 3. Top: Molecular structure of compound 3. Bottom: Labeled core of 3. Hydrogen bonds between the nonbridging oximate, azido ligands, and the coordinated water molecules are shown as red dashed lines.

Figure 4. Left: Molecular structure of compound 4. Right: Labeled core of 4. Hydrogen bond between the two nonbridging oximes is shown as a red dashed line.

Figure 5. Plot of the π-ring contacts between pyC{CN}NO– ligands for 1 (top left), 3 (bottom), and 4 (top right). The distances between the N atoms of the nitrile functions and the centroid of the pyridinic rings are plotted as red dashed lines.

Figure 6. Arrangement of the trimeric molecules of 1 by hydrogen bonds and π–π/lone-pair–π interactions along perpendicular directions.

Figure 7. Left: Plot of the intermolecular π–π and C–H/π-ring interaction between pyC{CN}NO– ligands in compound 4. Right: Cl–π-ring interaction of the dichloromethane solvent with the pyridinic ligands.

Figure 8. Left: Product of χMT versus T for compounds 1 (diamonds), 3 (circles), and 4 (squares). Right: Magnetization plot at 2 K for compounds 3 (circles) and 4 (squares). Solid lines show the best obtained fits.

Scheme 2. Coupling schemes for compounds 1 (left), 3 (center), and 4 (right).

Scheme 3. Core of the topology exhibited by 4. Ni–O–Ni (α) bond angles and Ni–N–O–Ni (τ) torsion angles are summarized in Table 5.

436 **Table 1.** Table 1. Selected distances [Å] and angles [°] of the core of compound 1.

437

Ni(1)–N(1)	2.071(3)	Ni(1)–N(3)	2.040(2)
Ni(1)–O(1)	2.042(2)	Ni(1)–O(4)	2.023(2)
Ni(1)–O(7)	2.100(2)	Ni(1)–O(9)	2.055(2)
Ni(2)–N(4)	2.086(3)	Ni(2)–N(6)	2.059(2)
Ni(2)–N(10)	2.115(3)	Ni(2)–N(12)	2.049(2)
Ni(2)–O(1)	2.064(2)	Ni(2)–O(5)	2.082(2)
Ni(3)–N(7)	2.060(2)	Ni(3)–N(9)	2.034(3)
Ni(3)–O(1)	2.024(2)	Ni(3)–O(2)	2.051(2)
Ni(3)–O(6)	2.071(2)	Ni(3)–O(8)	2.107(2)
Ni(1)–O(1)–Ni(2)	114.9(1)	Ni(1)–N(3)–O(2)–Ni(3)	14.6(2)
Ni(2)–O(1)–Ni(3)	114.0(1)	Ni(3)–N(9)–O(5)–Ni(2)	26.0(2)
Ni(1)–O(1)–Ni(3)	106.0(1)	Ni(2)–N(12)–O(4)–Ni(1)	4.7(3)
Ni(1)···Ni(2)	3.4601(7)	Ni(2)···Ni(3)	3.4280(6)
Ni(1)···Ni(3)	3.2478(7)		

438

439

440

441

442 **Table 2.** Selected distances [Å] and angles [°] for compound 2.

443

Ni–O(1)	2.030(6)	Ni–O(2)	2.029(6)
Ni–O(3)	2.013(6)	Ni–O(4)	2.041(6)
Ni–O(5)	2.034(5)	Ni–O(6)	2.024(6)
Na–O(1)	2.365(7)	Na′–O(2)	2.448(6)
Na–O(4)	2.431(6)	Na′–O(3)	2.350(6)
Na–O(5)	2.377(6)	Na′–O(6)	2.378(8)
Ni–O(1)–Na	112.22(6)	Ni–O(2)–Na′	112.22(6)
Ni–O(4)–Na	102.80(7)	Ni–O(3)–Na′	102.80(7)
Ni–O(5)–Na	102.80(7)	Ni–O(6)–Na′	102.80(7)
Ni···Na	3.014(4)	Ni···Na′	3.023(4)

444

445

446

447

448 **Table 3** Selected distances [Å] and angles [°] of the core of compound 3.

449

Ni(1)–N(1)	2.078(2)	Ni(1)–N(2)	2.027(2)
Ni(1)–N(4)	2.061(2)	Ni(1)–N(5)	2.047(2)
Ni(1)–N(13)	2.085(2)	Ni(1)–O(3)	2.059(1)
Ni(2)–N(7)	2.098(2)	Ni(2)–N(8)	2.064(2)
Ni(2)–N(10)	2.042(2)	Ni(2)–N(11)	2.063(2)
Ni(2)–N(13)	2.070(2)	Ni(2)–O(2)	2.125(1)
Ni(3)–O(1)	2.038(1)		
Ni(3)–O(3)	2.080(1)	Ni(1)–N(5)–O(2)–Ni(2)	26.6(2)
Ni(3)–O(5)	2.035(1)	Ni(1)–O(3)–N(8)–Ni(2)	26.5(2)
Ni(1)–O(3)–Ni(3)	112.22(6)	Ni(1)–N(2)–O(1)–Ni(3)	13.7(2)
Ni(1)–N(13)–Ni(2)	102.80(7)	Ni(2)–N(8)–O(3)–Ni(3)	104.2(1)
Ni(1)···Ni(2)	3.2466(5)	Ni(1)···Ni(3)	4.5218(6)
Ni(2)···Ni(3)	3.4357(5)		

450

451

452

453

454 **Table 4** Selected distances [Å] and angles [°] of the core of compound 4.

455

Ni(1)–N(1)	2.043(2)	Ni(1)–N(2)	2.105(2)
Ni(1)–N(4)	2.048(2)	Ni(1)–N(5)	2.072(2)
Ni(1)–O(4)	2.060(2)	Ni(1)–O(6)	2.125(2)
Ni(2)–N(7)	2.055(2)	Ni(2)–N(8)	2.002(2)
Ni(2)–N(10)	2.064(2)	Ni(2)–N(11)	2.003(2)
Ni(2)–O(2)	2.128(2)	Ni(2)–O(6)	2.129(2)
Ni(3)–N(13)	2.044(2)	Ni(3)–N(14)	2.136(3)
Ni(3)–N(15)	2.053(2)	Ni(3)–N(16)	2.069(2)
Ni(3)–O(2)	2.104(2)	Ni(3)–O(3)	2.078(2)
Ni(1)–O(6)–Ni(2)	98.29(6)	Ni(1)–O(4)–N(11)–Ni(2)	24.8(2)
Ni(2)–O(2)–Ni(3)	98.69(6)	Ni(3)–N(9)–O(5)–Ni(2)	26.0(2)
Ni(1)···Ni(2)	3.2176(6)	Ni(2)–N(8)–O(3)–Ni(3)	27.4(3)
Ni(2)···Ni(3)	3.2104(6)	Ni(1)–N(5)–O(2)–Ni(2)	25.8(2)
Ni(1)···Ni(3)	4.0016(7)	Ni(2)–O(6)–N(16)–Ni(3)	30.0(2)
		Ni(1)–N(5)–O(2)–Ni(3)	78.6(2)
		Ni(1)–O(6)–N(16)–Ni(3)	74.5(2)

456

457

458

Table 5. Magneto-structural parameters for the reported compounds with the core plotted in Scheme 3. The complexes from the literature[16] are named according to their CCDC codes. Bond and torsion angles were taken as average values.

	α	τ_1	τ_2	J_1	J_2	Ref.
4	98.49	26.10	75.35	–26.8	+2.0	–
BURSOX	99.92	32.83	72.45	–17.5	–10.5	[16a]
HOSWOB	100.51	37.28	72.56	–28.8	–15.2	[16b]
XASJEH	100.65	24.07	75.82	–16.4	–4.0	[16c]

Table 6. Crystal data, data collection and structure refinement details for the X-ray structure determination of compounds 1–4.

	1·2.5MeOH	**2**	**3**·2CH_2Cl_2	**4**·2CH_2Cl_2
Formula	$C_{69}H_{70}F_6N_{24}Ni_6O_{23}$	$C_{15}H_{12}F_9NaNiO_6$	$C_{58}H_{40}Cl_4N_{30}Ni_5O_{10}$	$C_{44}H_{29}BCl_4F_4N_{18}Ni_3O_6$
M_r	2069.75	540.95	1752.55	1310.59
System	triclinic	orthorhombic	triclinic	monoclinic
Space group	*P*1	*Fdd*2	*P*1	$P2_1/c$
a [Å]	9.826(2)	35.214(4)	11.460(2)	15.270(2)
b [Å]	12.578(2)	21.489(2)	11.682(2)	21.595(2)
c [Å]	17.631(3)	10.825(1)	14.791(2)	19.347(2)
α [°]	78.444(3)	90	104.465(5)	90
β [°]	89.925(3)	90	105.070(5)	127.433(6)
γ [°]	86.209(3)	90	103.814(5)	90
V [$Å^3$]	2130.2(7)	8191(2)	1750.9(4)	5066.0(9)
Z	1	16	1	4
T [K]	273(2)	100(2)	100(2)	100(2)
λ (Mo-K_α) [Å]	0.71073	0.71073	0.71073	0.71073
$\rho_{calcd.}$ [$g\,cm^{-3}$]	1.613	1.755	1.662	1.718
μ(Mo-K_α) [mm^{-1}]	1.398	1.079	1.552	1.398
R	0.0366	0.0598	0.0355	0.0384
wR^2	0.1072	0.1558	0.0963	0.1140

473 **Scheme 1.**

474

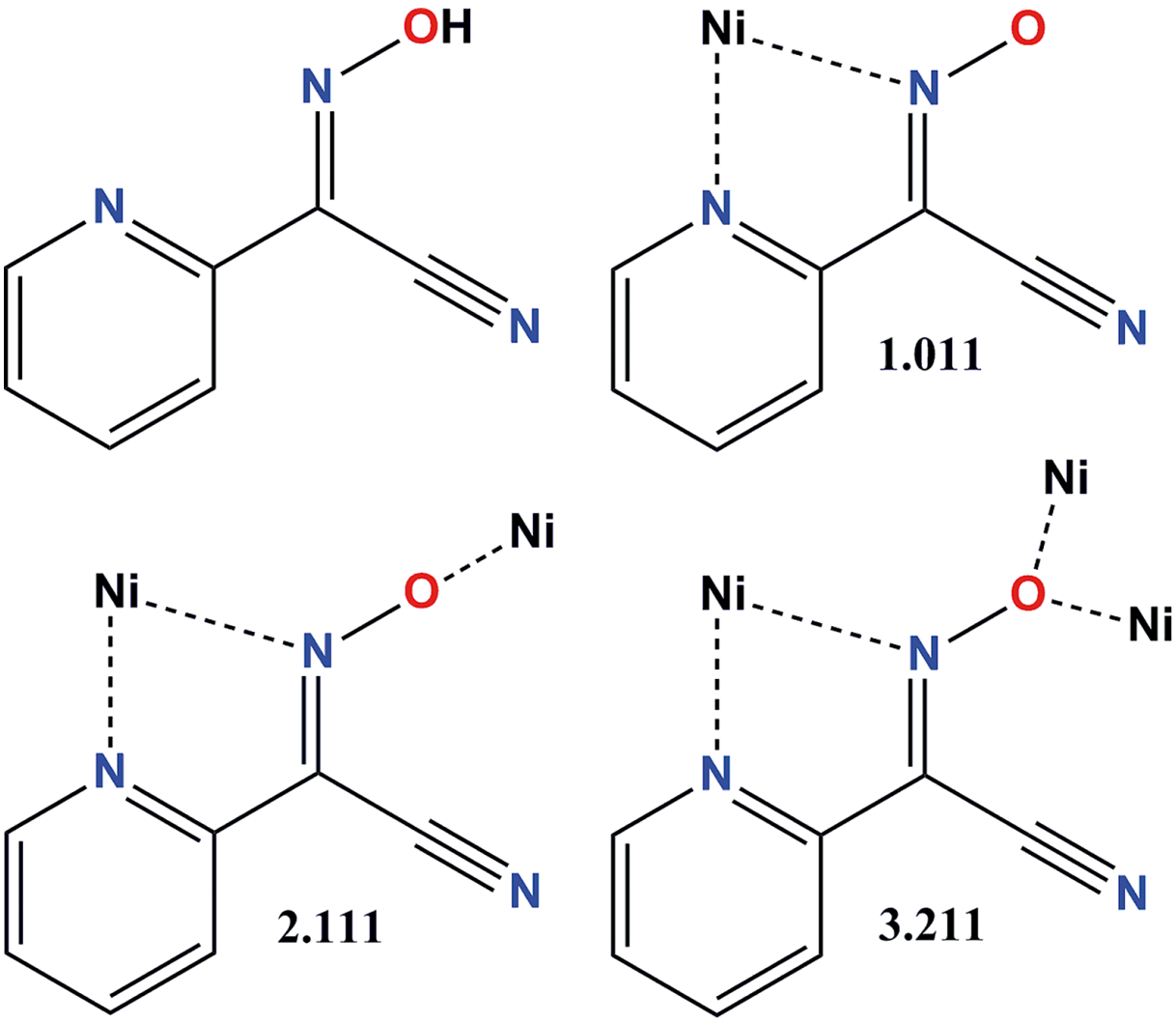

475

476

477

478

Figure 1

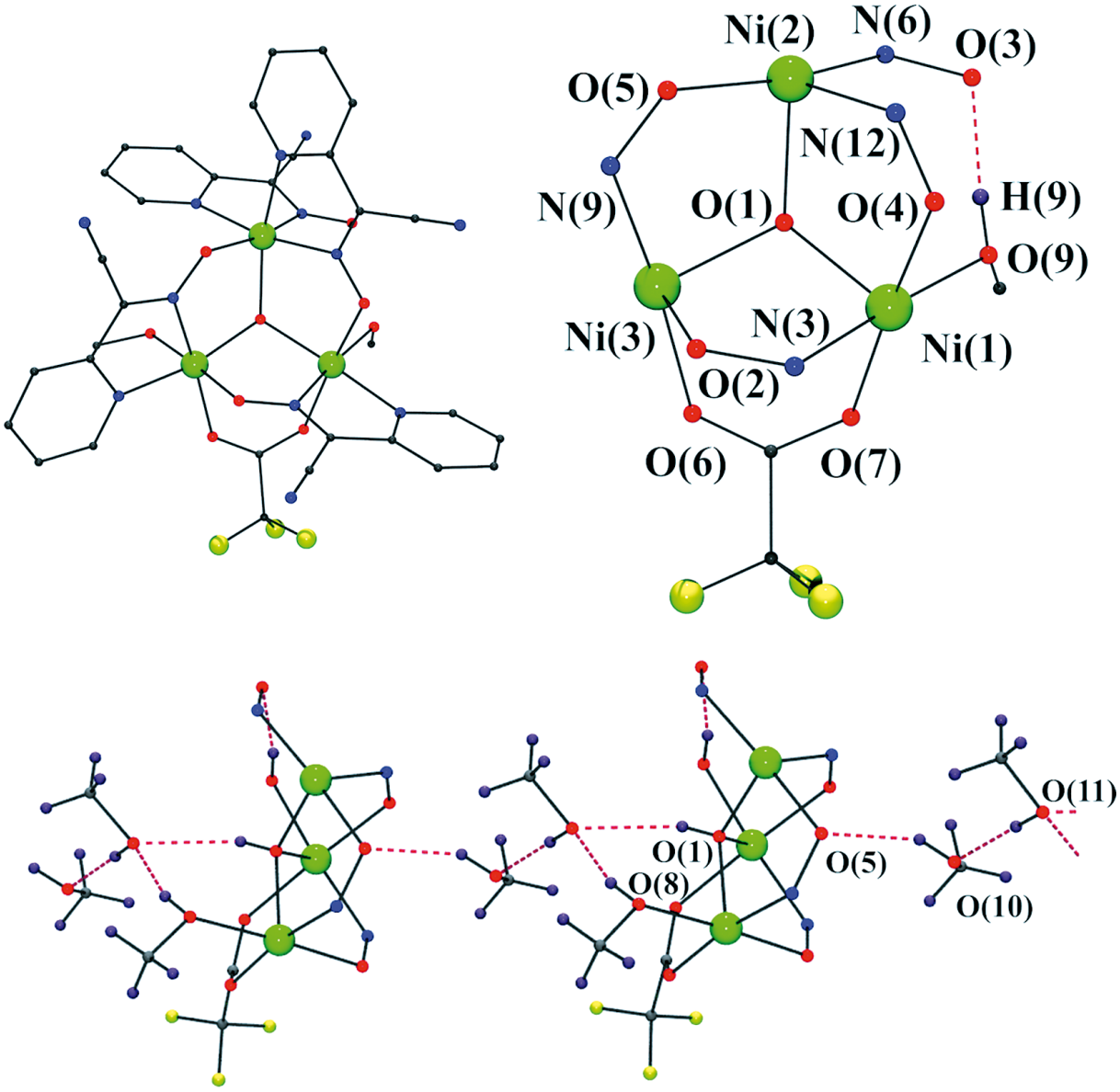

Figure 2

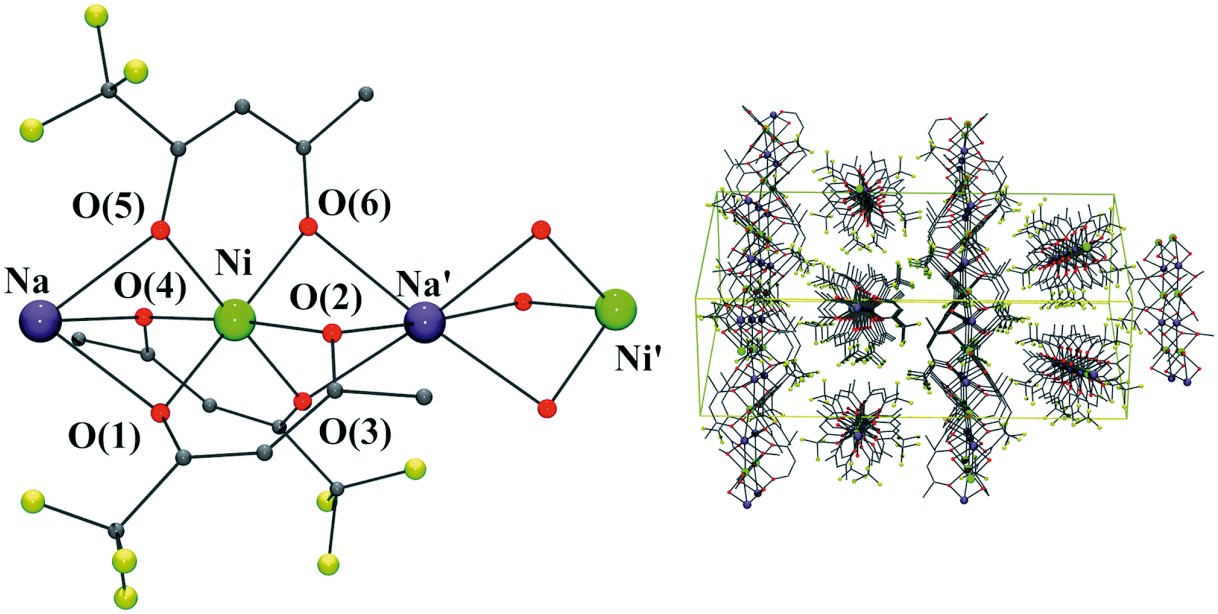

491 **Figure 3**

492

493

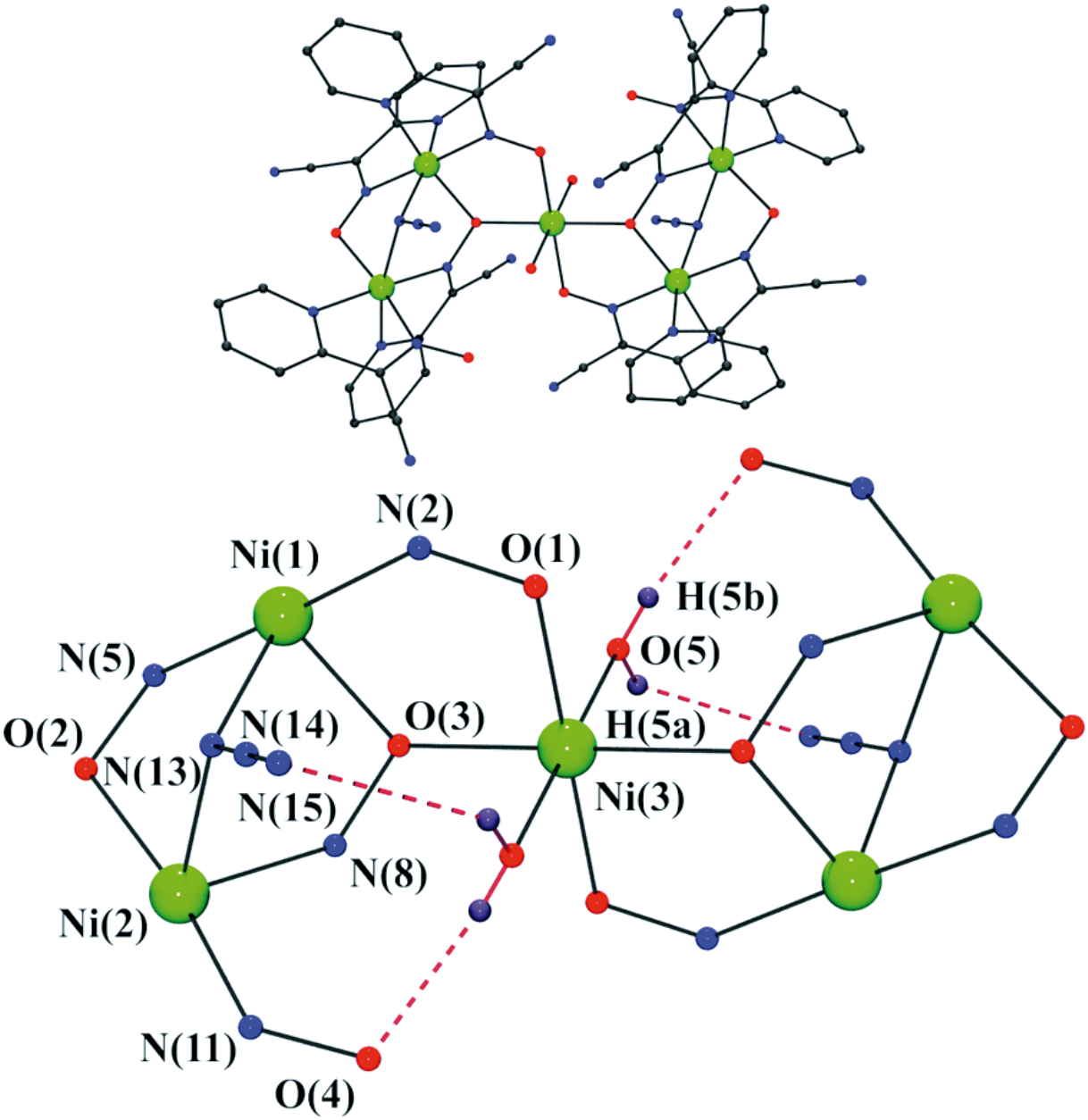

494

495

Figure 4

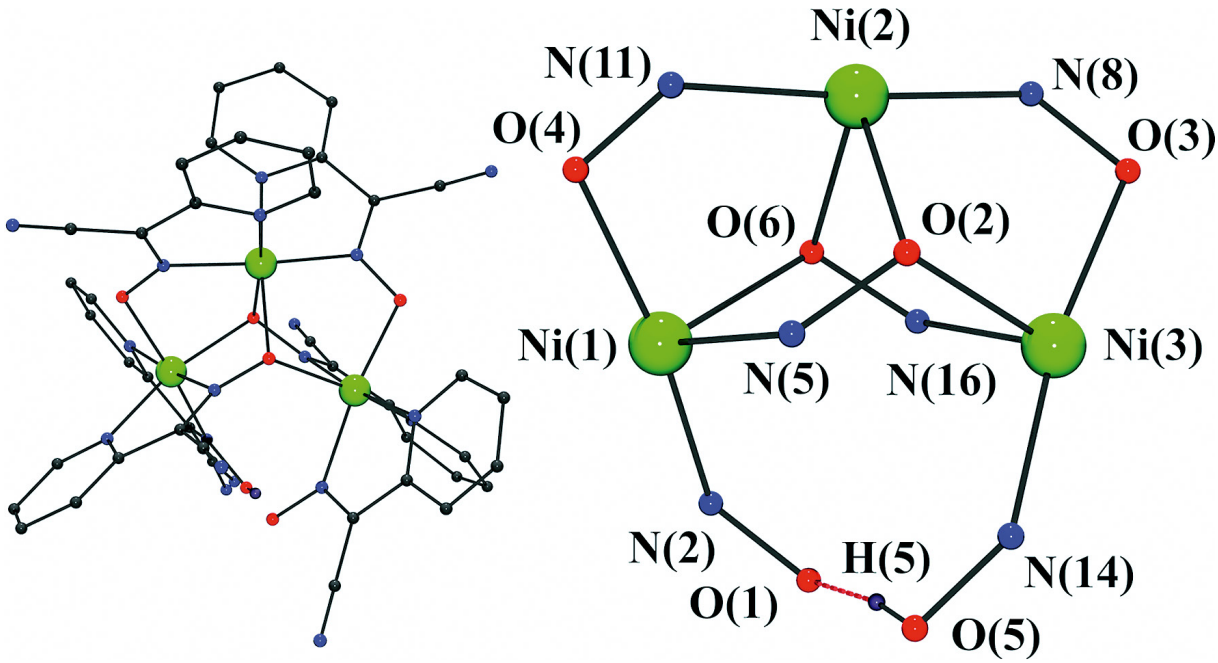

501 **Figure 5**

502

503

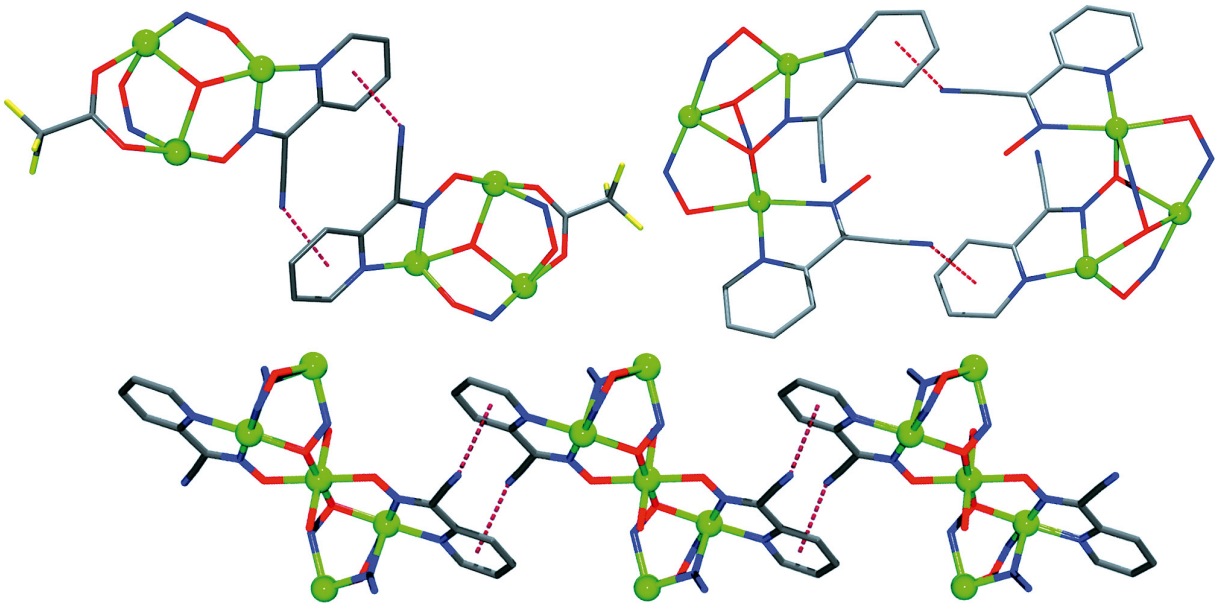

504

505

506 **Figure 6**

507

508

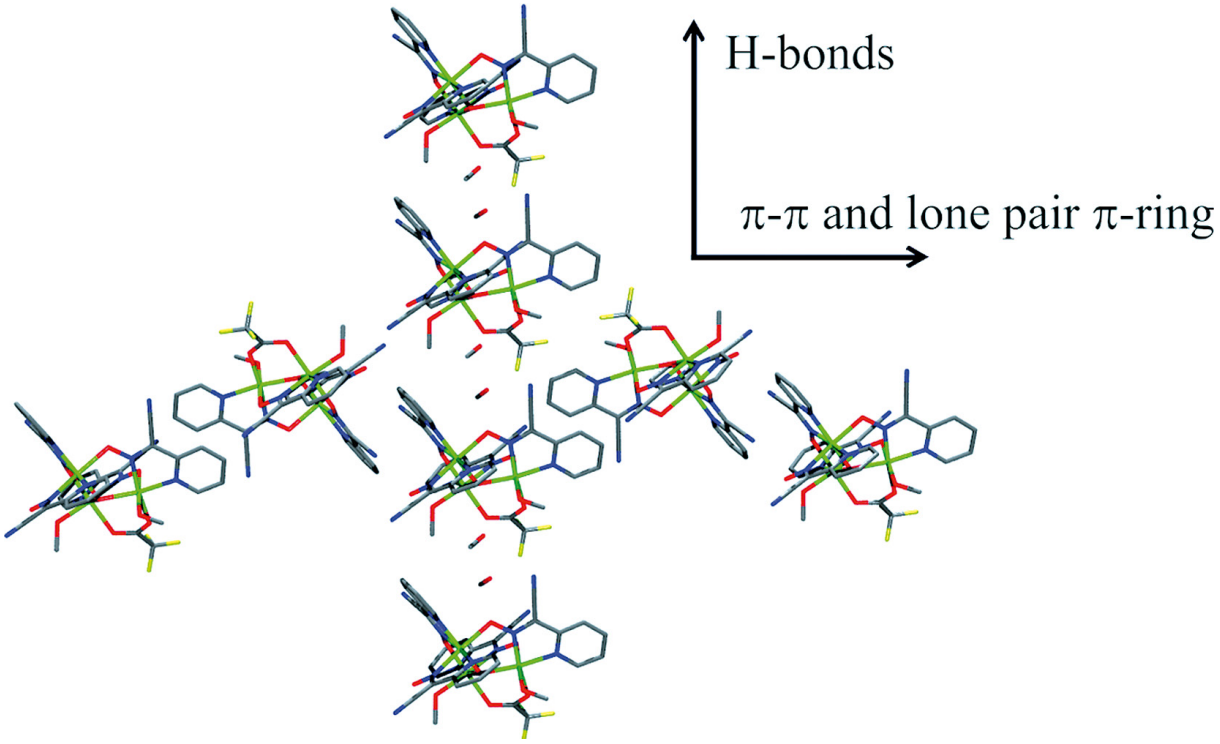

509

510

511

512 **Figure 7**

513

514

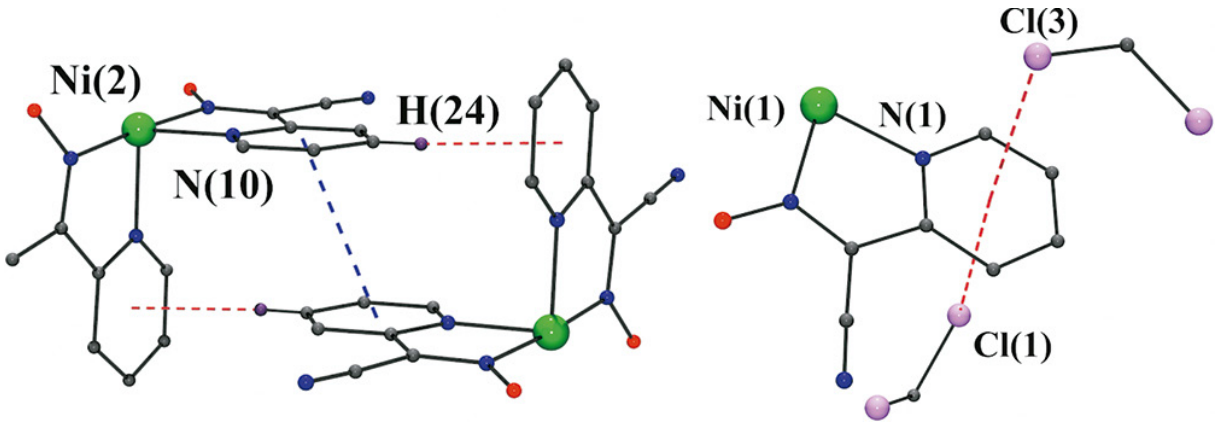

515

516

517 **Figure 8**

518

519

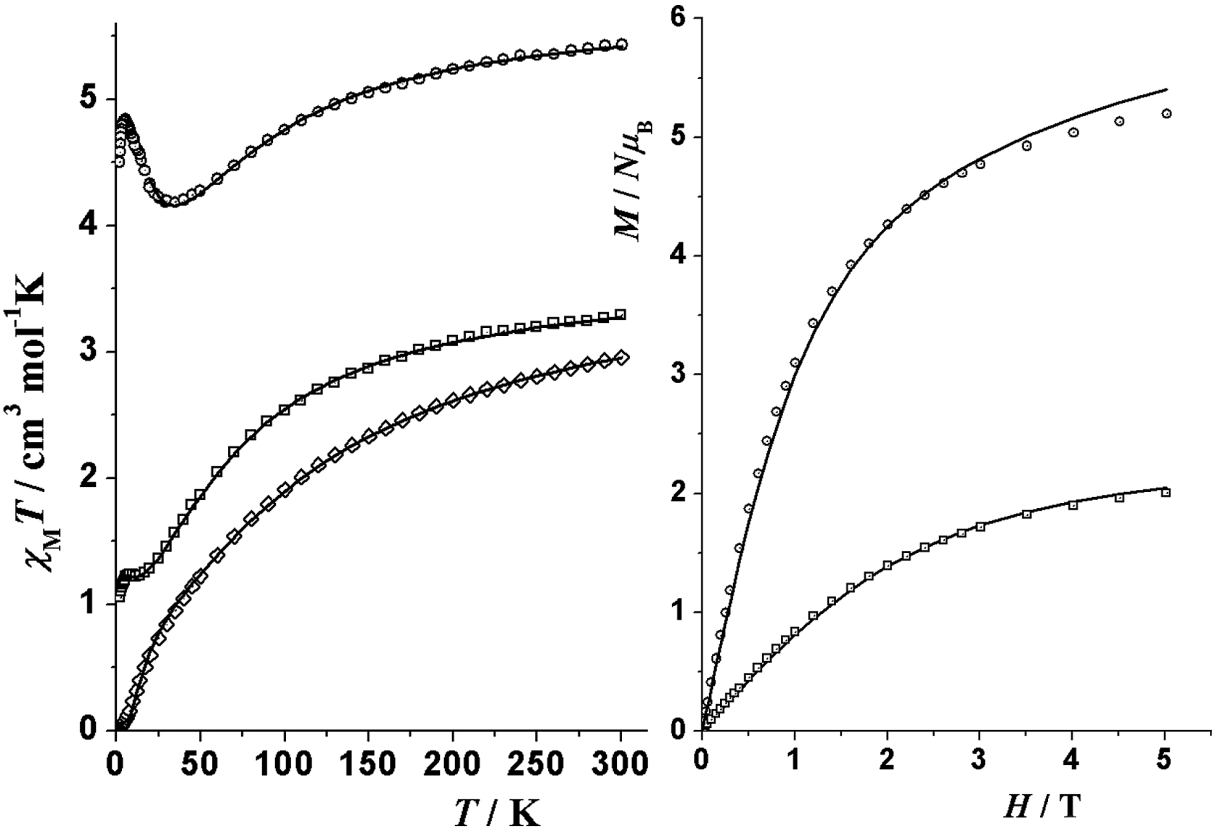

520

521

Scheme 2.

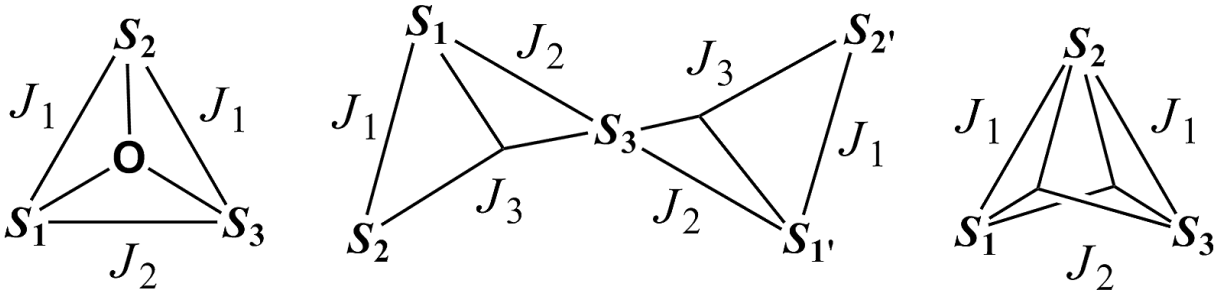

527 **Scheme 3.**

528

529

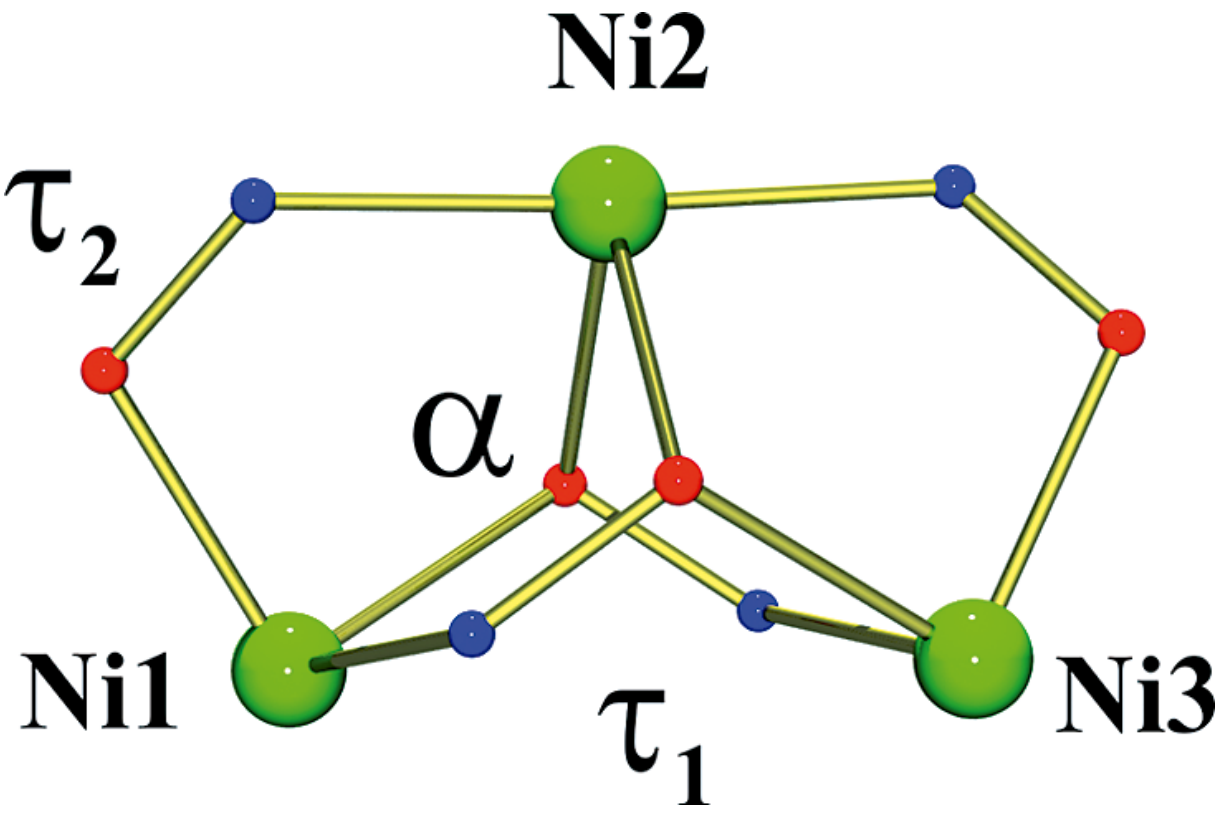

530